Nuclear Science and Techniques **22** (2011) 338–343

An analytical simulation technique for cone-beam CT and pinhole SPECT

ZHANG Xuezhu QI Yujin*

Shanghai Institute of Applied Physics, Chinese Academy of Sciences, Shanghai 201800, China

Abstract This study was aimed at developing an efficient simulation technique with an ordinary PC. The work involved derivation of mathematical operators, analytic phantom generations, and effective analytical projectors developing for cone-beam CT and pinhole SPECT imaging. The computer simulations based on the analytical projectors were developed by ray-tracing method for cone-beam CT and voxel-driven method for pinhole SPECT of degrading blurring. The 3D Shepp–Logan, Jaszczak and Defrise phantoms were used for simulation evaluations and image reconstructions. The reconstructed phantom images were of good accuracy with the phantoms. The results showed that the analytical simulation technique is an efficient tool for studying cone-beam CT and pinhole SPECT imaging.

Key words Computer simulation, Mathematical Phantom, Cone-beam CT, Pinhole SPECT

1 Introduction

Computer simulation is widely used in scientific research, product development and practical predictive applications[1–2], for validating and implementing image reconstruction methods, designing objective imaging systems, and evaluating image quality in especially radiology and nuclear medicine[3–4]. Along with the emerging pre-clinical molecular imaging techniques, such as micro-CT and micro-SPECT for *in vivo* small animal imaging, computer simulations are used to investigate high performance instrumentation before developing practical imaging systems.

As a statistical simulation method, Monte Carlo (MC) simulation is often used on an imaging system, but achieving quantitative accuracy of an MC simulation is time-consuming, and can only be realized with a computer of sufficiently high performance or parallel computer cluster. This study was aimed at developing an analytical simulation technique being effective and applicable on a PC for cone-beam CT and pinhole SPECT imaging. The mathematical derivation of imaging formation was investigated by analytical coordinate transformation and projection operation. The adaptive mathematical phantoms were designed and implemented for different imaging modalities and acquisition modes. The technique performances were evaluated and validated by phantom computational experiments and corresponding image reconstruction for cone-beam CT, single-pinhole SPECT with circular-orbit and helical-orbit scan modes, and multi-pinhole SPECT imaging.

2 Methods

2.1 General image formation modeling

X-ray CT imaging is based on detection of object-penetrating low energy photons generated by an X-ray tube, while a SPECT camera detects tissue-penetrating gamma photons emitted from concentrated radioactive tracer *in vivo*[5–7]. The formations of both the imaging modalities are approximately described as a continuous integral model by mathematical methods, and formulated as Eq.(1), which ignores degrading factors of attenuation, scattering, noise, etc.

$$P = \int_L f(x)\mathrm{d}x \tag{1}$$

Supported by National Natural Science Foundation of China (10875162)

* Corresponding author. *E-mail address*: qiyujin@sinap.ac.cn

Received date: 2011-08-01

For the integral calculation, the ray-tracing nominated as a term is regularly taken in image reconstruction and computer simulation. This method describes that the radiations transmit the object and their intersection are the tracing integral portion, which is the projection of the radial beam. Also, the mathematical methods of image formation could be approximately described as discrete projection equations, in which the imaging object is visualized as voxellated matrix. Eq.(2) is a brief discretized model for the projection procedure.

$$P = \sum_{j=1}^{M} C_j \bar{f}(\boldsymbol{x}) \tag{2}$$

According to the voxel-driven method for image reconstruction from projections of CT and SPECT, a projection is summation of photons about the transmission attenuation coefficient of CT or emission of radioactivity from the voxels of SPECT imaging object to the detector bins. We use the ray-tracing and the voxel-driven methods for practical implementation of image reconstruction and computer simulation in cone-beam CT and pinhole SPECT imaging.

2.2 Projection operators

The mathematical modelling of image formation and reconstruction for CT and SPECT refers to the coordinate transformation in specific imaging geometry. Assuming a rotating object and a stationary detector for the cone-beam CT and pinhole SPECT imaging, we can derive the projection operators in Cartesian coordinate systems[8–9] shown schematically in Fig.1, for the coordinate transformation, from an object reference system (O‴x‴y‴z‴) to a detector imaging reference system (Oxyz), which involves an angle rotation (θ) around the axis of rotation (AOR), a tilted angle rotation (α) from O‴x‴ to Ox, a screwed angle rotation (β) from O‴y‴ to Oy, and a coordinate translation (x_c, y_c, z_c). These can be described as Eq.(3), which are the four times multiplication of the operators $\boldsymbol{R}_\theta$, $\boldsymbol{R}_\alpha$, $\boldsymbol{R}_\beta$ and $\boldsymbol{T}$, and α, β and θ are assumed as clock-wise angle.

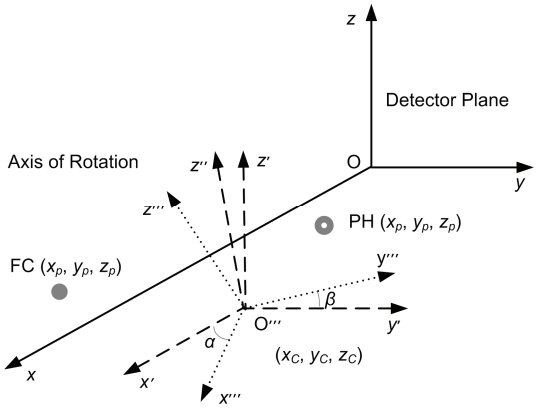

Fig.1 Schematics of coordinate transformation from an object reference system to a detector reference system for cone-beam CT and pinhole SPECT imaging.

$$\boldsymbol{R}_\theta = \begin{bmatrix} \cos\theta & \sin\theta & 0 & 0 \\ -\sin\theta & \cos\theta & 0 & 0 \\ 0 & 0 & 1 & 0 \\ 0 & 0 & 0 & 1 \end{bmatrix} \quad \boldsymbol{R}_a = \begin{bmatrix} \cos\alpha & 0 & \sin\alpha & 0 \\ 0 & 1 & 0 & 0 \\ -\sin\alpha & 0 & \cos\alpha & 0 \\ 0 & 0 & 0 & 1 \end{bmatrix} \quad \boldsymbol{R}_\beta = \begin{bmatrix} 1 & 0 & 0 & 0 \\ 0 & \cos\beta & -\sin\beta & 0 \\ 0 & \sin\beta & \cos\beta & 0 \\ 0 & 0 & 0 & 1 \end{bmatrix} \quad \boldsymbol{T} = \begin{bmatrix} 1 & 0 & 0 & x_c \\ 0 & 1 & 0 & y_c \\ 0 & 0 & 1 & z_c \\ 0 & 0 & 0 & 1 \end{bmatrix}$$

$$[x_\theta \quad y_\theta \quad z_\theta \quad 1] = \boldsymbol{T} \times \boldsymbol{R}_\beta \times \boldsymbol{R}_\alpha \times \boldsymbol{R}_\theta \times [x''' \quad y''' \quad z''' \quad 1]^T \tag{3}$$

The coordinate of focal center (FC) of X-ray tube or pinhole (PH) collimator is (x_p, y_p, z_p), with $x_p > x_c$ for cone-beam CT, and $x_p < x_c$ for pinhole SPECT.

The projection operators of cone-beam and pinhole imaging are derived in Eq.(4),

$$y_d = y + \left[\frac{x_d - x}{x - x_p}\right](y - y_p), \quad z_d = z + \left[\frac{x_d - x}{x - x_p}\right](z - z_p) \tag{4}$$

where, (x_d, y_d, z_d) denotes the projection coordinate of the object transmitted by the X-ray source or emitted through the pinhole collimator to the detector plane at $x_d = 0$.

2.3 Analytical phantom generations

The mathematical phantoms for computer simulation of radiological imaging can be divided into analytical and anthropomorphic phantoms involving stylized and

voxel-based modals[10]. Similar to MC methods, an anthropomorphic simulation needs too much computation for a PC to perform a practical task. Based on a geometrical model of ellipsoid or cylinder, analytical phantoms can be implemented with general computors. For our imaging studies, we developed several analytical phantoms including 3D Shepp-Logan, Hot-spot and Defrise phantoms as routine evaluation tools in computer simulation of CT and SPECT.

Based on ellipsoids of different sizes, 3D Shepp-Logan phantom was extensively used in the early CT study to simulate a human head approximately[11]. It can be described by Eq.(5), an analytical second-order quadratic equation,

$$\left(\frac{u'''-u'''_c}{a}\right)^2+\left(\frac{v'''-v'''_c}{b}\right)^2+\left(\frac{w'''-w'''_c}{c}\right)^2\le 1 \tag{5}$$

where, u''', v''' and w''' are the coordinate in object reference system (O$'''x'''y'''z'''$) introduced in Section 1.2; u'''_c, v'''_c, and w'''_c are the center position of a specific ellipsoid; and a, b, and c are the three corresponding axial radius.

The 3D Hot-spot Jaszczak phantom is based on hollow cylinders with channels of different diameters, and used for SPECT studies to evaluate reconstruction resolution of an imaging system.

The 3D Defrise phantom consisting of flat cylinders is used to evaluate an axial imaging resolution. The cylinder phantom can be described by Eq.(6), with its coordinate of height position (w) being constrained in [$-w'''_{\min}$, $w'''_{\max}$], which are coordinate of the bottom and top surfaces, respectively.

$$\left(\frac{u'''-u'''_c}{a}\right)^2+\left(\frac{v'''-v'''_c}{b}\right)^2\le 1,\ -w'''_{\min}\le w\le w'''_{\max} \tag{6}$$

The geometrical model may be positions at any direction, and a given position of the phantom in the object reference system O$'''x'''y'''z'''$ relates to another coordinate transformation similar to the derivation of Section 1.2, thus describing as the multiplication of the operators ($\boldsymbol{M}'''_{\varphi}$, $\boldsymbol{M}'''$, $\boldsymbol{M}'''_{\eta}$ and $\boldsymbol{T}'''$) in Eq. (7).

$$\boldsymbol{M}'''_{\phi}=\begin{bmatrix}\cos\phi & \sin\phi & 0 & 0\\ -\sin\phi & \cos\phi & 0 & 0\\ 0 & 0 & 1 & 0\\ 0 & 0 & 0 & 1\end{bmatrix}\quad \boldsymbol{M}'''_{\rho}=\begin{bmatrix}\cos\rho & 0 & \sin\rho & 0\\ 0 & 1 & 0 & 0\\ -\sin\rho & 0 & \cos\rho & 0\\ 0 & 0 & 0 & 1\end{bmatrix}\quad \boldsymbol{M}'''_{\eta}=\begin{bmatrix}1 & 0 & 0 & 0\\ 0 & \cos\eta & -\sin\eta & 0\\ 0 & \sin\eta & \cos\eta & 0\\ 0 & 0 & 0 & 1\end{bmatrix}\quad \boldsymbol{T}'''=\begin{bmatrix}1 & 0 & 0 & u'''_c\\ 0 & 1 & 0 & v'''_c\\ 0 & 0 & 1 & w'''_c\\ 0 & 0 & 0 & 1\end{bmatrix}$$

$$[x''' \quad y''' \quad z''' \quad 1]=\boldsymbol{T}'''\times\boldsymbol{M}'''_{\eta}\times\boldsymbol{M}'''_{\rho}\times\boldsymbol{M}'''_{\phi}\times[u''' \quad v''' \quad w''' \quad 1]^T \tag{7}$$

For the computer simulation implemented by ray-tracing method, the projections are generated by the intersecting distances which are solved with the source trajectory function and the geometrical phantom function. For the voxel-driven method, the projections are summed by the weighted voxel values of the phantom in the imaging region.

In practice, the ray-tracing algorithm is utilized to implement the computer simulation of CT imaging; and the voxel-driven algorithm, to implement the computer simulation of pinhole SPECT imaging with collimator detector response blurring[12]. The statistical distribution and noise degrading in the projections are incorporated after the analytical simulation procedure.

3 Simulation results

To test the analytical simulation techniques, we performed a series of phantom computer simulations for cone-beam CT, single-pinhole SPECT, with adaptive scan modes and multi-pinhole SPECT imaging. The image reconstruction algorithms we developed include Feldkamp algorithm[13], 3D pinhole OS-EM algorithm[9,14] with circular and helical scans, and 3D multi-pinhole OS-EM algorithm.

3.1 Cone-beam CT simulation

A mathematical 3D Shepp−Logan phantom was used to evaluate performance of image reconstruction algorithms in early CT studies. The phantom is super-positioned by 10 ellipsoids of different densities and sizes[2]. Fig.2(a) shows the trans-axial image of the computerized phantom, with a 3D perspective rendering image in Fig.2(b). The noise-free projections were generated by ray-tracing method, and acquired

by 128×128 detector bins and 120 angular views over 360° circular-orbit scan with a magnitude 2.5 of focal-length/ROR. Fig.2(c) shows a sample projection, no degrading factors such as statistical fluctuation scatter and noise effects were considered in the CT simulation, and the data were reconstructed using Feldkamp algorithm. As a comparison, Fig.2(d) shows a reconstructed trans-axial image of the same slice of the phantom in Fig.2(a). It can be seen that the analytical ray-tracing algorithm provides a flexible and efficient computer simulation for the image reconstruction of CT imaging.

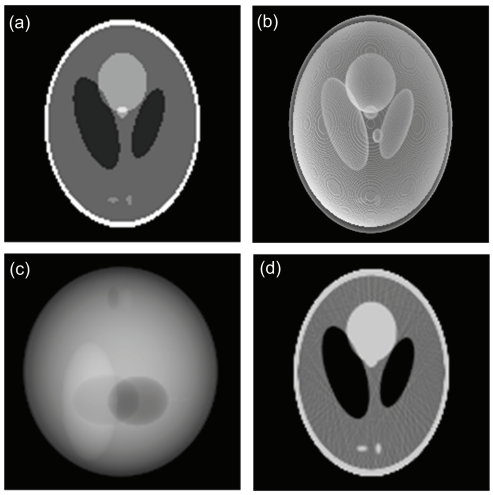

Fig.2 Computer simulation of a 3D Shepp−Logan phantom for cone-beam CT. (a) Sample trans-axial slice image. (b) 3D perspective rendering image. (c) Sample projection image by ray-tracing algorithm. (d) Reconstructed trans-axial image by Feldkamp algorithm.

3.2 Single-pinhole SPECT simulation

To test the reconstruction algorithms designed for pinhole SPECT imaging, phantom simulations were performed to evaluate the trans-axial reconstructed resolution with circular scan and the axial reconstructed resolution with helical scan. The simulation imaging parameters were based on the micro-SPECT system developed by our group[8].

A mathematical 3D Jaszczak phantom was used for the pinhole SPECT simulations. As shown in Fig.3(a), the phantom contains six sets of hot spot channels in diameters of 2.4, 2.0, 1.7, 1.35, 1.0 and 0.75 mm. Fig.3(b) shows a sample projection of the phantom imaged by the micro-SPECT. We present the 3D perspective rendering of the developed mathematical phantom in Fig.3(c). In Fig.3(d), the noise-free projections are generated by voxel-driven algorithm with 1.0 mm keel-edge pinhole collimator, and blurred further with Poisson statistical distribution and noise contaminated. No scattering and attenuation effects were considered in this simulation. The data were acquired by 70×70 detector bins and 90 angular views over 360° scans with 35-mm ROR(radius of rotation), and the projection data were reconstructed by 3D pinhole OS-EM algorithm. Fig.3(e) shows the trans-axial image, and Fig.3(f), the OS-EM reconstructed images of the simulated projections. They are of better validity than the practical imaging, to approach the real imaging system for the reconstruction algorithm.

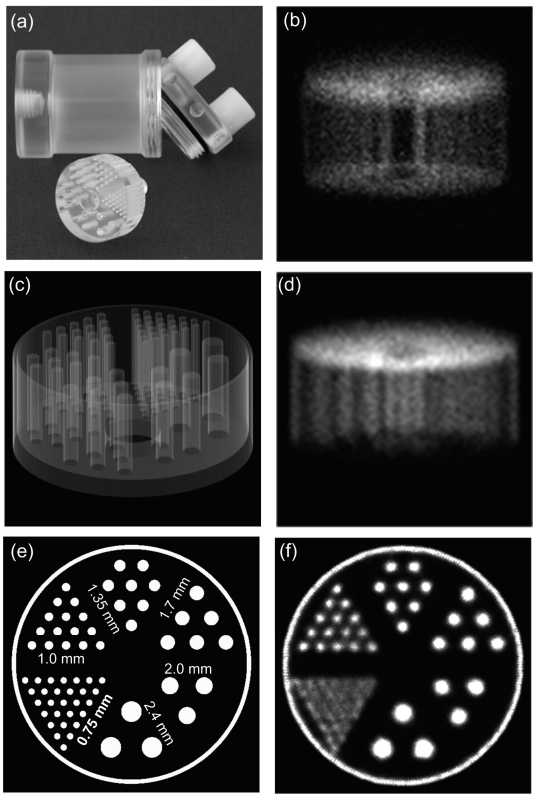

Fig.3 Computer simulation of 3D Hot-spot phantom for circular single-pinhole SPECT. (a) Jaszczak phantom. (b) Projection image by μ-SPECT. (c) 3D perspective rendering of the mathematical phantom. (d) Projection image with keel-edge pinhole collimator response and statistical noise blurring. (e) Trans-axial slice image of the phantom. (f) Reconstructed trans-axial image by 3D pinhole OS- EM algorithm.

Also, a mathematical 3D Defrise phantom was used to test the simulation and reconstruction algorithm for pinhole SPECT with helical scan mode. The phantom (Fig.4a) consists of seven cylindrical disks to simulate the interlayer hot activity solutions. The sample projections of practical phantom imaged

by the micro-SPECT are given in Fig.4(b). The 3D perspective rendering of the mathematical phantom are shown in Fig.4(c). The noise-free projections were generated by voxel-driven algorithm with 1.0 mm keel - edge pinhole collimator detector response and further statistical noise blurring. No scatter and attenuation effects were considered in this simulation. The projection data were acquired by 70×70 detector bins with 37 mm ROR and simulated by 180 angular views over 720° using helical scan of 0.15 mm pitch. The simulated sample projections are shown in Fig. 4(d), with the data being reconstructed by the 3D pinhole OS-EM algorithm we developed. The simulated central axial slice image is shown in Fig.4(e), and the reconstructed image in Fig.4(f), demonstrating that our developed simulation technique can be an efficient tool for the helical reconstruction algorithm implementation which improves the axial spatial resolution of reconstruction image.

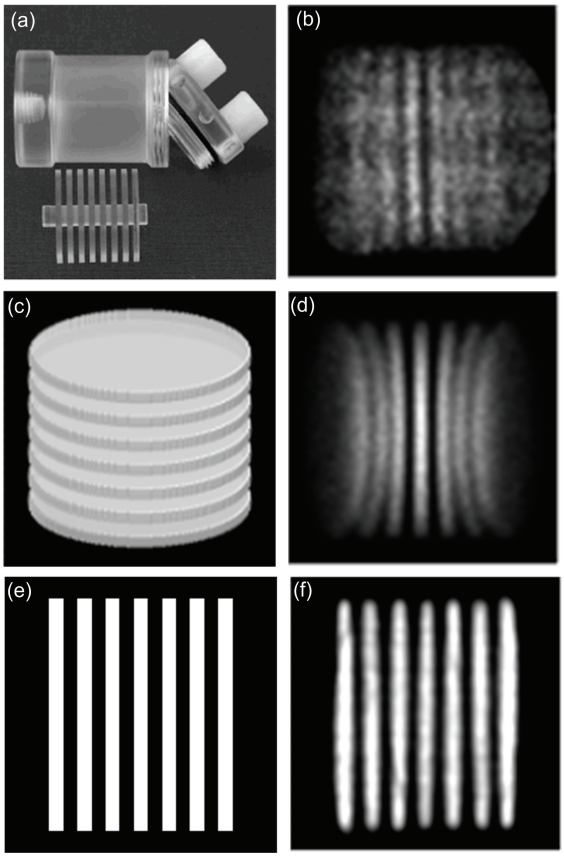

Fig.4 Computer simulation of 3D Defrise phantom for helical single- pinhole SPECT. (a) Defrise phantom. (b) Projection image by μ-SPECT. (c) 3D perspective rendering of the mathematical phantom. (d) Sample projection image with keel-edge pinhole collimator response and noise blurring. (e) Central axial slice of the phantom. (f) Central axial image reconstructed by helical 3D OS-EM algorithm.

3.3 Multi-pinhole SPECT simulation

The analytical multi-pinhole SPECT computer simulation algorithm provides sufficient projection sampling. Seven knife-edge pinhole collimators of 0.6-mm aperture diameter are configured at different horizontal and vertical positions. The 3D Hot-spot and Defrise phantoms in Section 3.2 were used in the multi-pinhole SPECT imaging simulations.

Figure 5(a) shows a sample projection of the simulated 7 pinhole SPECT imaging with 3D Hot-spot phantom. The noise-free projections were generated by knife-edge pinhole collimator response and Poisson statistical noise blurring without considering any scattering and attenuation effects. The data were acquired by 120×120 detector bins and 45 angular views over 360° scans with 35-mm ROR. The projection data were reconstructed by the 3D multi-pinhole pinhole OS-EM algorithm. Fig.5(b) shows the OS-EM reconstruction image of the simulated projections.

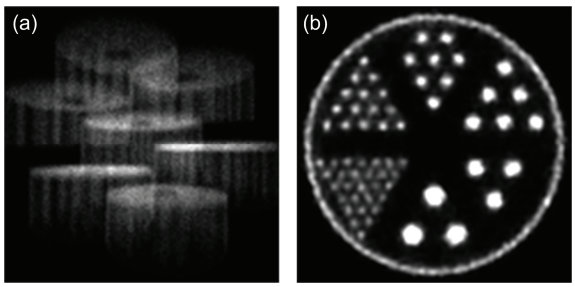

Fig.5 Computer simulation of 7-pinhole SPECT for 3D Jaszczak phantom imaging. (a) Sample projection image with keel-edge pinhole collimator response and statistical noise blurring. (b) Trans-axial reconstruction image by 3D multi-pinhole OS-EM algorithm.

Figure 6(a) shows a sample projection of the 3D Defrise multi-pinhole SPECT imaging simulated by noise-free analytical computation with knife-edge pinhole collimator response and statistical blurring. The projection data were simulated by 120×120 detector bins with 40 mm ROR and 30 angular views over 360° scans. We implemented 3D multi-pinhole OS-EM algorithm to reconstruct the projection data. The central axial reconstructed image is shown in Fig. 6(b). The results demonstrate that this simulation technique provide an efficient tool for evaluation of system design and reconstruction algorithms implementation for multi-pinhole SPECT imaging.

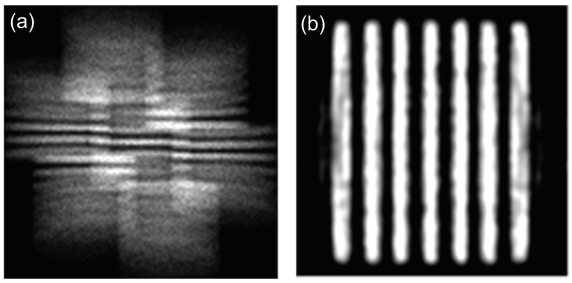

Fig.6 Computer simulation of 7-pinhole SPECT for 3D Defrise phantom imaging. (a) Sample projection image with keel-edge pinhole collimator response and statistical noise blurring. (b) Central axial reconstruction image by 3D multi-pinhole OS-EM algorithm.

4 Conclusions

We have developed the efficient analytical computer simulation techniques for cone-beam CT, single-pinhole SPECT with different scan mode and multi-pinhole SPECT imaging. Their performances were compared with the practical experimental phantom imaging, and evaluated by our developed reconstruction algorithms. The results show that our developed analytical simulation algorithms with ray-tracing method for cone-beam CT image computation, and voxel-driven method for pinhole SPECT image computation with degrading blurring and adaptive scan modes could provide good projection data for the evaluation of imaging system and reconstruction algorithms. Our analytical simulation technique is an efficient for studying cone-beam CT and pinhole SPECT imaging.

References

1 Rubinstein R Y. Simulation and the Monte Carlo method, Wiley-New York, 1981.

2 Raeside D E. Monte Carlo principles and applications, Phys Med Biol 1976, **21:** 181–197.

3 Zaidi H. Med Phys, 1999, **26:** 574-608.

4 Rogers D W O. Phys Med Biol, 2006, **51:** R287–R301.

5 Herman G T. Fundamentals of computerized tomography: Image reconstruction from projections, Academic Press, 1980.

6 Kak A C, Slaney M. Principles of computerized tomographic imaging, IEEE Press, 1988.

7 Barrett H H, Mayer K J. Foundations of image science, Wiley-Interscience, 2003.

8 Zhang X Z, Chen F F, Qi Y J, *et al.* Proc IEEE Nucl Sci Symp Conf Rec, 2009, 3318–3321.

9 Zhang X Z, Qi Y J. Chin Sci Bull, 2011, **56:** 340–348.

10 Zaidi H, Tsui B M W. Proceedings of the IEEE, 2009, **97:** 1935–1937.

11 Yang M, Lang T, Wei Y. Acta Armamentarii, 2006, **27:** 437–441.

12 Zhang X Z, Dai Q S, Qi Y J. Proc IEEE Nucl Sci Symp Conf Rec, 2008, 5255–5259.

13 Feldkmap L A, Davis L C, Kress J W. J Opt Soc Am Al, 1984, 612–619.

14 Hudson H M, Larkin R S. IEEE Trans Med Imaging, 1994, **13:** 601–609.